Angewandte Chemie 119 2007) 7465 –7468

Role of Lattice Strain and Defects in Copper Particles on the Activity of $Cu/ZnO/Al_2O_3$ Catalysts for Methanol Synthesis

I. Kasatkin[1], P. Kurr[1], B. Kniep[2], A. Trunschke[1*], R. Schlögl[1]

[1]Department of Inorganic Chemistry, Fritz-Haber-Institute of the MPG, Faradayweg 4-6, 14195 Berlin, Germany
[2]Süd-Chemie AG R&D Catalysts, Waldheimer Str. 13, 33052 Bruckmühl (Germany

[*] Corresponding author: e-mail trunschke@fhi-berlin.mpg.de,

Received: June 14, 2007 Revised: July 26, 2007.

Keywords: aluminum, copper, electron microscopy, methanol synthesis, zinc

Copper-based catalysts are industrially applied in various reactions including water-gas shift, synthesis of fatty alcohols from fatty acid methyl esters, and methanol synthesis. Today, methanol is produced at low pressures (35-55 bar) and 200-300°C over $Cu/ZnO/Al_2O_3$ catalysts.[1] Due to the great commercial relevance, Cu/ZnO-based catalysts have been extensively studied and many different models have been proposed regarding the nature of active sites and the valence of copper under conditions of methanol formation, such as Cu^{1+} dispersed in ZnO,[2,3] metallic copper supported on ZnO,[4] dynamic surface and bulk alloy formation depending on the reduction potential of the synthesis gas,[5,6] Cu^- at the so-called Schottky junction between metallic Cu and the semiconductor ZnO,[7] and ZnO segregated on Cu^{1+}.[8] The catalytic activity of the binary catalyst has been reported to be several orders of magnitude greater than that of metallic Cu or pure ZnO, respectively, indicating a synergetic interaction of the two components.[9] ZnO is regarded either as provider of atomic spillover hydrogen for further hydrogenation of adsorbed reaction intermediates on Cu sites,[10,11] or as a structure directing support controlling dispersion, morphology, and specific activity of the metal particles.[12-18] Strong interaction between the metal and the support, especially in the case of large lattice mismatch, is known to cause strain in the metal particles, to which an increase in catalytic performance has been attributed.[19-21] On the other hand, 1-ML-high and thicker Cu islands epitaxially grown on the ZnO (000 $\bar{1}$) surface were experimentally found to be strain-free.[22]

In most of the earlier studies model catalysts with low Cu loadings (Cu/Zn << 1) containing large ZnO single crystals have been investigated, although, usually, in commercial catalysts copper represents the main component (Cu/Zn > 1) and the ZnO particles, acting rather as a spacer than as a support, are comparable in size, or even smaller than the Cu particles. In this paper we report the results of TEM and in situ XRD characterization of a series of $Cu/ZnO/Al_2O_3$ catalysts exhibiting different catalytic activities. The molar ratio Cu:Zn:Al = 60:30:10 is characteristic of commercial catalysts.[1] The microstructural features of the materials prepared by coprecipitation with sodium carbonate from metal nitrate solution are analyzed after calcination in air at 330°C and subsequent reduction in hydrogen at 250°C. A quantitative estimation of imperfections in metal particles determined by combination of independent TEM and in situ XRD investigations is established. The implications of strain in Cu crystallites and the defect frequency associated therewith on the catalytic activity of $Cu/ZnO/Al_2O_3$ catalysts in methanol synthesis are discussed.

The TEM and HRTEM images shown in Figure 1 illustrate the microstructure typical of the catalysts studied. Generally, 10 to 15 clusters similar to the one shown in Figure 1a, which had the size that varied from 100 nm to several micrometers, were analyzed in each of the catalysts with Energy-Dispersive X-Ray spectroscopy (EDX) to determine the concentrations of Al, Cu, and Zn. The average value (Al: 10.6 ±4.5 at.%; Cu: 62.7 ±7.2 at.%; Zn: 26.7 ±4.2 at.%) is close to the nominal composition. Figure 2 that contains data of all catalysts illustrates the scattering due to local inhomogeneities.

The particles of Cu and ZnO form an irregular framework (Figure 1b). The particles of ZnO, which are comparable in size or smaller than the Cu particles, serve as spacers between the latter, preventing them from sintering.

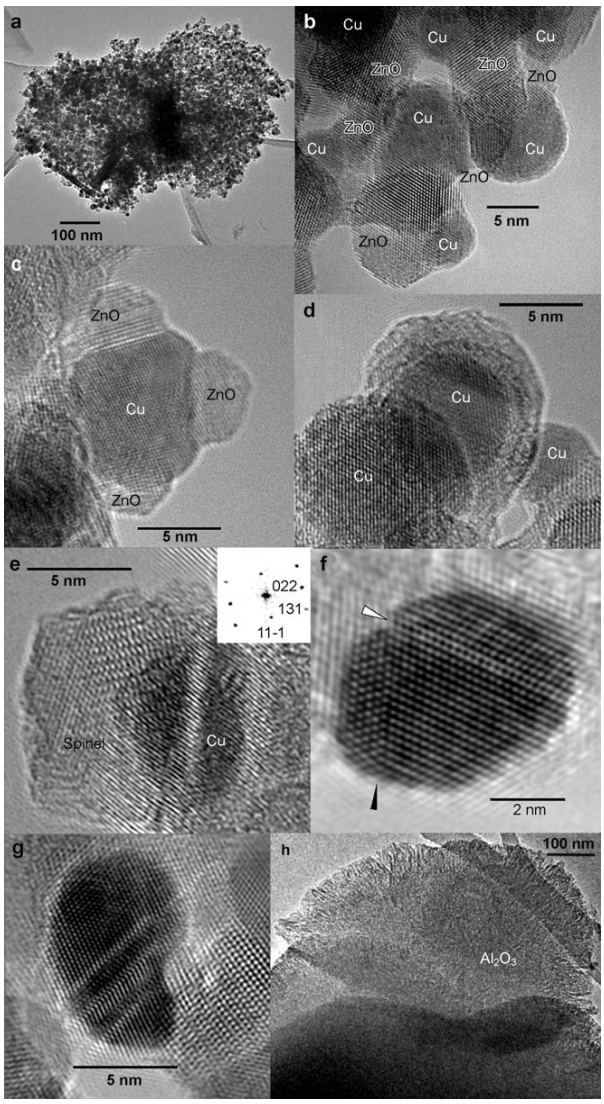

Figure 1: Microstructural features revealed with TEM and HRTEM. See comments in the text.

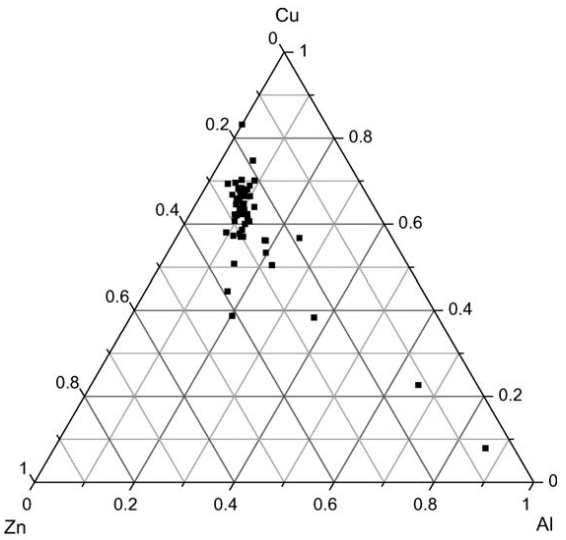

Figure 2: Elemental distribution determined by EDX analyses

Frequently, the Cu particles are in contact with several ZnO particles. It occurs that the copper surface is partially or completely covered by ZnO (Figure 1c and d) and, thus, less accessible to the reacting molecules. As evident from the images in Figure 1, most of Cu particles have a rounded (non-equilibrium) shape, similar to that of an ellipsoid or sphere, sometimes truncated with {111} or {100} facets. The mean Cu particle size was determined by measuring projected areas of individual particles in the TEM images and calculating the equivalent diameter, which corresponds to the diameter of a circle having the same area. Statistical tests showed that the mean sizes were significantly different in different analyzed clusters, and depended on the elemental composition (data not shown). Redundant measurements were performed in order to check that further increase in the number of measured particles changed neither the mean size, nor the shape of distribution curve. The total number of measured particles varied from 5060 to 24200 in different samples. Because of lower degree of crystallinity of ZnO and Al_2O_3 compared to that of Cu, the oxide particles were not well shaped and separated from one another. This disallowed comparably accurate determination of their mean size in TEM projections.

Figure 3a demonstrates that a relation between the mean Cu particle size measured by TEM (open squares) and the catalytic activity in methanol synthesis is missing. Based on the results of EDX analyses and the particle size measurements the mean specific Cu surface area was determined in each of the samples studied (Figure 3a, open triangles). In those calculations the effect of decreasing fraction of open surface with decreasing particle size due to the stronger wetting of small particles was taken into account, but not the coverage of Cu surface by smaller ZnO particles (Figure 1c and d). Accurate determination of gas-accessible Cu surface area using two-dimensional TEM projections was impossible. However, consistent copper surface areas have been measured by N_2O chemisorption for two of the catalysts. Therefore the values based on TEM are considered to be representative for the copper surface areas accessible to the gas phase. As expected, the calculated mean surface area is inversely proportional to the mean particle size. A correlation between copper surface area and catalytic activity is not observed, albeit, the most active catalyst possesses the highest surface area and vice versa.

As seen in Figure 3b, with the exception of the most active material, the degree of asymmetry (skewness) and the kurtosis of the particle size distribution decrease with increasing catalytic activity. In other words, with increasing activity the particle size distribution approaches the Gaussian law. A pronounced Log-normality, i.e., asymmetry of the particle size distribution measured with TEM may result from sintering of smaller Cu particles, which, in turn, may be considered as an indication of the non-optimal microstructure of the material. As seen in the Figure 3b, more symmetric size distribution results in increased activity; on the other hand, a material with asymmetric distribution

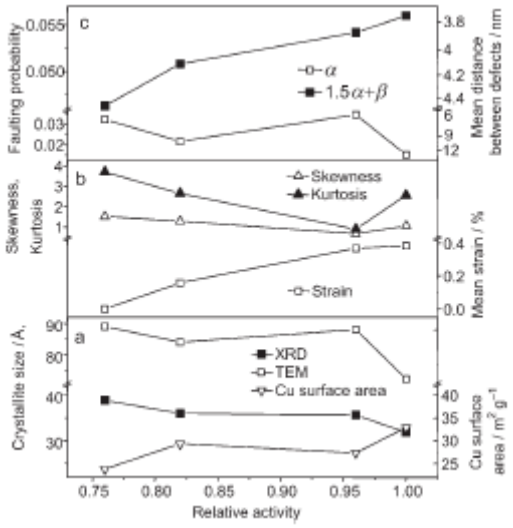

Figure 3. Microstructural parameters obtained with TEM and XRD as a function of relative catalytic activity in methanol synthesis. The standard errors for the mean particle size determined with TEM are within the size of the corresponding symbols.

demonstrated the highest activity, which could be associated with considerably smaller mean Cu particle size and, correspondingly, higher specific Cu surface area. However, ineffective interaction with the spacing ZnO resulted in a higher tendency towards sintering in the latter material.

Alumina tends to segregate implying its restricted ability to act as dispersing agent. Agglomerated masses of amorphous material comparable in size with clusters of Cu/ZnO nanoparticles but containing only traces of Cu and Zn were observed (Fig. 1 h). In addition, amorphous or poorly crystallized alumina was intermixed with Cu and ZnO particles. In rare cases, HRTEM images reveal small regions of better crystallized particles (Figure 1e). The corresponding power spectrum (Figure 1e, inset) allowed identification of a spinel-like cubic structure with the lattice distances d_{111}, d_{311}, d_{220} markedly closer to those of $ZnAl_2O_4$ (ICDD 5-669) than of pure cubic Al_2O_3 (ICDD 47-1292). Positive correlations between the concentration of Al and Zn determined with EDX in different clusters within all samples support the hypothesis on the formation of $ZnAl_2O_4$ spinel.

Most of the Cu particles, especially those larger than 5 nm, contained various defects, among which the most typical were twins and stacking faults (Figure 1 e-g). Many particles demonstrated multiple twinning along a certain octahedral plane (Figure 1g), but only a few decahedral and no icosahedral cyclic twins were found. Characteristically, most of the twin boundaries were only partially coherent, i.e., the regular close packing of the octahedral planes was interrupted by missing a layer in the direction normal to the twin boundary. Coherent and partially coherent twin boundaries are marked in Fig. 1 f with the black and white arrows, correspondingly.

The profiles of the Cu 111 and 222 reflections measured by in situ X-ray diffraction were analyzed within the 2θ intervals of 38-49 and 90-100 deg, respectively, after the neighboring peaks had been fitted with pseudo-Voigt functions and their contributions subtracted. A comparison with the XRD pattern of LaB_6 (NIST standard SRM 660a) obtained under the same conditions has shown that the effect of size/strain peak broadening dominated over the instrumental effect to such a degree that the latter could be safely neglected.

An adopted model was used to simulate the peak profiles from the first principles by double summation of interference functions over different column lengths and over different lattice spacings according to the corresponding distribution functions.[23] A trial-and-error procedure was used to determine approximate values, which were further refined with a least square procedure in the final step. As opposed to similar models,[24] the applied model did not impose any restrictions on the laws of both lattice spacing and crystallite size distribution (Normal, LogNormal, etc): The size distribution shape was described by a polynomial function whose coefficients were refined during simulation. The flexibility in defining non-standard or polymodal size distributions allowed highly precise simulation of the XRD peak shape.

To evaluate both crystallite size and strain, the profiles of the 111 and 222 reflections of Cu were simulated simultaneously with the same set of model parameters. Strain was introduced into the model as a Gaussian distribution of the interplanar distances about the mean value of d_{111} = 2.088 Å. The standard deviation of the distribution expressed in percent of d_{111} was used as a quantitative measure of strain. The values plotted in Figure 3b should only be considered as relative values based on a rough estimation. Comparison of the mean crystallite size calculated from diffraction peak broadening (Figure 3a, filled squares) with the particle size measured with TEM (Figure 3a, open squares) shows that the former were invariably smaller than the latter. The presence of stacking faults and twin boundaries in the particles (Figure 1f-g) may account for the discrepancy.[25] The stacking fault probability α could be determined from the measurements of intervals between the adjacent peaks in the XRD patterns in such pairs as 111-200, which are known to progressively shift in opposite directions as α increases, and comparing them to the corresponding intervals in a "perfect" material using equations given by Warren.[25]

Accordingly, the stacking fault probability α was found to change in the series of studied materials as shown in Figure 3c. The right-hand axis in the figure shows the mean distance between the defects calculated as $l = d_{111}/\alpha$ or $l = d_{111}/(1.5\alpha+\beta)$, where β is the twinning probability. The overall faulting probability $1.5\alpha+\beta$ could be estimated from the comparison of apparent crystallite sizes determined by the shape analysis of different peaks. However, the low signal-to-noise ratio of XRD reflections other than 111 made their detailed analysis unreliable. Therefore, a combined analysis of XRD and TEM data has been un-

dertaken, which is based on the assumption that the presence of stacking faults and twin boundaries is the only reason for the smaller domain size measured by XRD compared to the mean particle size determined by TEM. In addition, a nearly spherical shape of the Cu particles is assumed, which is supported by the TEM images (Figure 1). The upper curve in Figure 3c shows the trend in the overall faulting probability in the studied catalysts obtained by the combined treatment of the series of TEM and XRD data.

Inspection of Figure 3 shows that the stacking fault probability α does not correlate with the activity, but changes in parallel with the TEM particle size, whereas the mean distance between stacking faults is comparable with the mean particle size (8.1 nm and 8.3 nm, respectively). This does not necessarily imply that there is a physical reason preventing small particles from faulting. The effect can be interpreted from a geometrical point of view: At a given mean distance between the defects, the larger particles contain defects with higher probability than the smaller ones.

At the same time, the independent measurements show that the activity scales with the overall faulting probability $1.5\alpha+\beta$. Since the methods of determination of $1.5\alpha+\beta$ and α were different, the twin boundaries imaged with HRTEM were often incoherent (faulted), and the geometric interpretation given in the previous paragraph might be wrong, the conclusion on the dominating role of twin boundaries in increasing activity may be doubtful. Nevertheless, the activating role of defects – without differentiation – seems to be obvious.

Moreover, the activity was found to scale with the strain in Cu crystallites (Figure 3b). The parallelism between the mean strain and the overall faulting probability does not allow distinguishing between the effects of specific atomic configurations which the twin boundaries and stacking faults produce on the surface of metal particles and of the strain itself, which is associated with these defects, but it clearly shows the essential role of imperfections in the Cu lattice for the increased activity of $Cu/ZnO/Al_2O_3$ catalysts in methanol synthesis.

In summary, the statistically meaningful analysis of the nanostructure of a series of methanol synthesis catalysts with a composition close to technical systems has revealed that the abundance of non-equilibrium structures in Cu, such as planar defects and strain, two properties which are strongly interrelated, clearly correlate with the catalytic activity. The families of correlations suggested by Muhler[26] may find their physical interpretation in the distribution functions of nanostructural properties as evidenced in Figure 3. We speculate at this point that the relevant non-equilibrium structure of active Cu is generated during synthesis explaining the phenomenon of "chemical memory".[27] The kinetic stabilization of metastable structures during long-term operation is seen as the physical reason of the kinetic "synergy" as was already suggested much earlier.[11] The synthesis procedures of Cu-based catalysts can now be redesigned optimizing their exact chemical composition (Figure 2), Cu particle size distribution function (Figure 3) and the abundance of stabilizing species at Cu interfaces (Figure 1). In parallel, the geometric and the surface electronic structure of highly active systems will be analyzed with synchtrotron-based techniques to further refine the structural properties of the active Cu metal phase under reaction conditions.

Experimental Section

A Philips CM200FEG microscope operated at 200 kV and equipped with a field emission gun and the Gatan imaging filter was used. The coefficient of spherical aberration was C_s = 1.35 mm. The information limit was better than 0.18 nm. High-resolution images with a pixel size of 0.016 nm were taken at the magnification of 1083000× with a CCD camera, and selected areas were processed to obtain the power spectra (square of the Fourier transform of the image). The power spectra (PS) were used for measuring interplanar distances (± 0.5 %) and angles (± 0.5 deg) for phase identification.

The XRD data in the 2θ range of 10 – 100 degree was collected on a STOE Theta/theta X-ray diffractometer. (CuKα radiation, secondary graphite monochromator, scintillation counter, 2 θ step 0.04 deg, counting time 5 sec) equipped with an Anton Paar XRK 900 in situ reactor chamber. The in situ reduction was performed at 250°C (heating rate 2°C/min) in 2%H2/N2.

The catalysts have been tested at a temperature of 483K and a pressure of 60 bar. The feed was composed of 72%H_2, 10%CO, 4%CO_2 and 14%He.

Acknowledgement

The authors are grateful to Prof. Dr. Thorsten Ressler, Technical University Berlin for fruitful discussions. We acknowledge the Federal Ministry of Education and Research for financial support (FKZ 01RI0529).

References

1] P.J.A. Tijm, F.J. Waller, D.M. Brown, Appl. Catal. A **2001,** *221*, 275-282.
[2] K. Klier, Adv. Catal. 1982, 31, 243-313.
[3] V. Ponec, Surf. Sci. 1992, 272, 111-117.
[4] K.C. Waugh, Catal. Today 1992, 15, 51-75.
[5] N.-Y Topsøe, H. Topsøe, Top. Catal. 1999, 8, 267-270.
[6] Y. Choi, K. Futagami, T. Fujitani, J. Nakamura, Appl. Catal. A 2001, 208, 163-167.
[7] J.C. Frost, Nature 1988, 334, 577-580.
[8] W.P.A. Jansen, J. Beckers, J.C. v. d. Heuvel, A.W. Denier v.d. Gon, A. Bliek, and H.H. Brongersma, J. Catal. 2002, 210, 229-236.
[9] R.G. Herman, K. Klier, G.W. Simmons, B.P. Finn, J.B. Bulko, J. Catal. 1979, 56, 407-429.
[10] R. Burch, S.E. Golunski, M.S. Spencer, J. Chem. Soc., Faraday Trans. 1990, 86, 2683-2691.
[11] M.S. Spencer, Catal. Lett. 1998, 50, 37-40.

[12] J. Yoshihara, C.T. Campbell, J. Catal. 1996, 161, 776-782.
[13] C.V. Ovesen, B.S. Clausen, J. Schiøtz, P. Stoltze, H. Topsøe, and J.K. Nørskov, J. Catal. 1997, 168, 133-142.
[14] T. Fujitani, J. Nakamura, Catal. Lett. 1998, 56, 119-124.
[15] N.-Y. Topsoe, H. Topsoe, J. Mol. Catal. A 1999, 141, 95-105.
[16] J.D. Grunwaldt, A.M. Molenbroek, N.-Y. Topsøe, H. Topsøe, B.S. Clausen, J. Catal., 2000, 194, 452-460.
[17] P.L. Hansen, J.B. Wagner, S. Helveg, J.R. Rostrup-Nielsen, B.S. Clausen, H. Topsøe, Science, 2002, 295, 2053-2055.
[18] R.A. Hadden, B. Sakakini, J. Tabatabaei and K.C. Waugh, Catal. Lett. 1997, 44, 145-151.
[19] M. M. Günter, T. Ressler, B. Bems, C. Büscher, T. Genger, O. Hindrichsen, M. Muhler, R. Schlögl, Catal. Lett., 2001, 71, 37-44.
[20] M. M. Günter, T. Ressler, R. E. Jentoft, B. Bems, J. Catal., 2001, 203, 133-149.
[21] J.B. Wagner, P.L. Hansen, A.M. Molenbroek, H. Topsøe, B.S. Clausen, S.J. Helveg, Phys. Chem. B 2003, 107, 7753-7758.
[22] N. Jedrecy, S. Gallini, M. Sauvage-Simkin, R. Pinchaux, Phys. Rev. B 2001, 64, 085424.
[23] I.A. Kasatkin, T.I. Ivanova, Crystallography Reports 1998, 43, 1015-1019.
[24] F.Sánchez-Bajo, A.L.Ortiz, F.L.Cumbrera, Acta Materialia 2006, 54, 1–10.
[25] Warren, B.E., X-ray Diffraction (New York: Dover Publications), 1990.
[26] M. Kurtz , N. Bauer , C. Büscher , H. Wilmer , O. Hinrichsen , R. Becker, S. Rabe , K. Merz , M. Driess , R. A. Fischer, M. Muhler, Catal. Lett. 2004, 92, 49-52.
[27] B. Bems, M. Schur, A. Dassenoy, H. Junkes, D. Herein, R. Schlögl, Chem. Eur. J. 2003, 9, 2039-2052.